electronics

Article

Study on the Design of Series-Type All-DC Wind Farms Based on Half-Bridge Voltage Balancing Circuits

Xiaochen Su [1], Haiyun Wang [1,*], Zhanlong Li [2] and Qianyu Ma [1]

[1] College of Electrical Engineering, Xinjiang University, Urumqi 830047, China; 107552201539@stu.xju.edu.cn (X.S.); 107552201507@stu.xju.edu.cn (Q.M.)
[2] Beijing Goldwind Science & Creation Wind Power Equipment Co., Ltd., Beijing 100176, China; lizhanlong@goldwind.com.cn
* Correspondence: why@xju.edu.cn

Abstract: Offshore wind farms connected in series, with each wind turbine connected in series with one another, enhance the coupling between them. Significant differences in wind speeds between neighboring DC wind turbines (DCWTs) might result in a substantial disparity in the output voltage, hence posing a risk of overvoltage. Nevertheless, implementing voltage-limiting configurations for DCWTs might lead to the dissipation of wind energy, thereby diminishing the wind farm's capacity to deliver electricity. This work introduces a half-bridge voltage balancing circuit (HVBC) topology as a solution to the issue of DCWT output voltage changes affecting the stable operation of wind farms. The proposed HVBC topology is designed specifically for large-capacity series-connected all-DC wind farms where wind speed variations occur. This design achieves power decoupling for series-connected all-DC wind farms by providing current compensation to the series-connected DCWTs. A control strategy is devised by examining the decoupling principle and operational characteristics of the HVBC. A 60 kV/48 MW tandem-type all-DC wind farm model consisting of six DCWTs in series is built in Matlab/Simulink. The model is then simulated to evaluate its performance under conditions of unequal wind speed, rapid changes in wind speed, and wind turbine failure shutdown. This research verifies the feasibility of the HVBC topology and improves the stability of the series-type all-DC wind farm.

Keywords: series-connected all-DC wind farm; half-bridge voltage balancing circuit; current compensation; power decoupling; modular DC/DC converter

check for updates

Citation: Su, X.; Wang, H.; Li, Z.; Ma, Q. Study on the Design of Series-Type All-DC Wind Farms Based on Half-Bridge Voltage Balancing Circuits. *Electronics* **2024**, *13*, 3839. https://doi.org/10.3390/electronics13193839

Academic Editors: Mohamed Benbouzid, Sinisa Durovic, Xiandong Ma and Hao Chen

Received: 27 August 2024
Revised: 23 September 2024
Accepted: 27 September 2024
Published: 28 September 2024

1. Introduction

Wind energy is a highly clean and eco-friendly form of energy. Due to the growing scarcity of land resources, the advancement of offshore wind power has emerged as a crucial route for the future development of wind power [1–3]. Aggressively advancing the development of offshore wind power is a crucial step towards achieving the "dual-carbon" objective and transitioning to renewable energy sources. The Global Wind Energy Council's (GWEC) Global Wind Power Report 2024 states that a total of 117 GW of new wind power was installed worldwide in 2023, resulting in a cumulative installed capacity of 1 TW [4]. A total of 10.8 GW of offshore wind power was installed, contributing to a cumulative installed capacity of 75.2 GW [4]. The advancement of offshore wind power towards deep and distant seas with increased capacity has rendered the traditional method of AC energy pooling and transmission ineffective due to issues such as reactive current and overvoltage. Consequently, the construction of all-DC wind farms, utilizing DC pooling and transmission, has emerged as the primary direction for the future development of offshore wind power [5–7].

Wind power systems in the DC domain can be classified into parallel and series types based on the manner of pooling energy [8–10]. Series-connected all-DC wind power systems raise the voltage level to the transmission voltage by connecting DCWTs in series with each other [11]. However, the arrangement of individual DCWTs in a wind farm in a series of connections intensifies the coupling between them, resulting in the degradation of the autonomous control of each DCWT [12,13]. The decoupling of control for series-connected all-DC wind farms is highly important for the coordinated control of DCWTs and the establishment of voltage restrictions for DCWTs to avoid overvoltage occurrences [14]. There are two main approaches to solving the DCWT output voltage balance in series-connected all-DC wind farms.

The first method is by limiting the voltage or limiting the power [15,16]. When the voltage across the DCWTs reaches a limit value, it is not increased, or when the output power of the DCWTs reaches a limit value, it is not increased. In [17], voltage fluctuations are suppressed by adding energy storage at the DC bus to absorb high-frequency power fluctuations. In [18], the range of DC bus voltage fluctuations is limited by transient rotor power feedback. However, after limiting the DC bus voltage, the current saturation characteristic caused during grid faults leads to transient instability [19]. The authors of [20,21] in the literature initially analyzed the coupling characteristics between DC wind turbines in series-type full-DC wind farms. They also explored the control methods for wind turbines in series-type DCWTs operating under voltage-limited conditions. This method, though, ensures that the DCWT is not at risk of overvoltage and avoids damage to the DCWT under unstable wind speed conditions. However, this method must give up part of the wind energy when limiting the voltage or limiting the power, resulting in part of the wind energy being wasted and also limiting the power generation capacity of the DCWT. The literature in [22] describes how the DC bus voltage and output power of each DCWT are regulated by adjusting the reference unit's mode to ensure equal values for each DCWT. This approach potentially mitigates the impact of the interconnection properties of DC wind farms that are connected in series. However, its effectiveness strongly depends on the operational condition of the reference unit, and the stability of the wind farm operation is compromised. In their studies, the authors of [23,24] suggested a strategy for controlling the speed of a series-connected DCWT to mitigate wind abandonment. This strategy involves storing and releasing energy through the rotor of the wind turbine. However, a limitation arises when the wind turbine reaches its maximum speed, as the rotor is unable to store any more energy, failing the variable speed control. The authors of [25] proposed the use of a DC collector to mitigate the impact of power fluctuations from wind turbines on their output voltage. However, the stabilizing effect of the wind turbine outlet voltage is not evident. While the solutions effectively mitigate the risk of series-connected DCWT overvoltage through voltage-limiting control, they significantly decrease the usage of wind energy. In addition, with the increase in the installed capacity of wind farms, the impact of common mode voltage on wind turbines cannot be ignored [26].

The second method is to provide a compensation current to the series-type DCWT by controlling the shunt circuit [27], which realizes the maximum power-tracking of the wind turbine in the case of wind speed inconsistency and ensures voltage balance at the machine end. However, this scheme is difficult to adapt to the direction of the large-scale and large-capacity development of offshore wind farms due to the limitation of the voltage stress of the switching devices in the shunt circuit. In their study, the authors of [27] introduced a novel configuration for connecting multiple DC wind farms in series. This configuration allows for the efficient tracking of maximum power from wind turbines, even in situations where wind speeds are not consistent. Additionally, it ensures that the voltage at the output of the wind turbines remains balanced by managing the shunt circuits to compensate for any current variations. Nevertheless, this solution is difficult to adapt to the development direction of large-scale and large-capacity offshore wind farms, and new solutions need to be researched.

This research presents a solution to the above issues by introducing a half-bridge voltage balancing circuit (HVBC) topology and its corresponding control method for high-capacity series-connected all-DC wind farms. Additionally, the working principle of this topology is thoroughly analyzed. The design of an all-DC wind farm, capable of operating reliably under varying wind speeds, has been completed based on this topology. Furthermore, the viability of the half-bridge voltage balancing circuit has been confirmed by simulation.

The rest of this article is structured as follows. Section 2 describes the topology of HVBC and its role in series-type all-DC wind farms. Section 3 analyzes the working principle of HVBC in terms of its operating status in different situations. Section 4 describes the control strategy of an HVBC-based series-type full-DC wind farm. Section 5 performs a simulation and discusses the simulation results. Section 6 concludes the paper.

2. Design Solutions for All-DC Wind Farms Connected in Series

2.1. Series-Connected All-DC Wind Farm Topology Based on HVBC

The conventional offshore wind farm is connected in series and operates on DC. It comprises DCWTs directly connected in series. Owing to the nature of the series circuit, the current flowing out of each DCWT connected in series is the same, resulting in a significant relationship between the output voltage and output power of the DCWT. The output power of each DCWT is mostly determined by wind speed. When the wind speed is equal, or the difference in wind speed is minimal, each wind turbine can achieve the same or similar DCWT output power by adjusting the pitch angle. This allows the export voltage of each DCWT to reach the same or a similar level, ensuring that the series-type all-DC wind farms operate smoothly. Nevertheless, if the wind speed discrepancy in a series-connected all-DC wind farm is significant, the DCWTs cannot achieve the desired similarity in outlet voltage by altering their pitch angle. Under these circumstances, the voltage exerted on the DCWTs will be greater when wind speeds are higher than when wind speeds are lower. This increased voltage can potentially result in DCWT failures.

The relationship between the output power and output voltage of a traditional series-type all-DC wind farm with n DCWTs can be expressed as

$$i_{\text{DC}} = \frac{P_1}{U_{\text{wt1}}} = \frac{P_2}{U_{\text{wt2}}} = \cdots = \frac{P_{n-1}}{U_{\text{wt}(n-1)}} = \frac{P_n}{U_{\text{wt}n}} \tag{1}$$

where i_{DC} is the output current of the series-connected all-DC wind farm, and P_i and $U_{\text{wt}i}$ are the output power and output voltage of the i th DCWT, respectively.

Equation (1) demonstrates that the output power of each DCWT in the series-type all-DC wind farm is exactly proportional to the output voltage. Therefore, the $U_{\text{wt}i}$ value of the i th DCWT can be represented as

$$U_{\text{wt}i} = \frac{P_i}{\sum\limits_{i=1}^{n} P_i} U_{\text{DC}} \tag{2}$$

where U_{DC} is the output voltage of the all-DC wind farm, the value of which is controlled by the onshore converter station. Consequently, the output voltage of the DCWT depends on its power level.

The output power of a wind turbine directly correlates to the wind speed at its location under the management of maximum power tracking. The variation in wind velocity at the precise location of each wind turbine inside a wind farm results in a disparity in the generated power of each turbine. When there is a significant power difference, the difference in the output voltage of the wind turbines increases accordingly. This can result in overvoltage issues for wind turbines operating at higher wind speeds, potentially causing damage and posing a serious threat to the safe and stable operation of wind farms. To address overvoltage in wind turbines resulting from wind speed variations, current research has primarily focused on implementing voltage-limiting control for wind turbines connected in series. This approach enhances the safety of wind turbine operation but also results in significant wind energy wastage.

This study presents a solution to the overvoltage issue in series-connected DC wind turbines caused by varying wind speeds. The proposed solution is a half-bridge voltage-balancing circuit for large-capacity series-connected all-DC wind farms. This topology achieves power decoupling for all-DC wind farm series-connected configurations at the DCWT port. It further stabilizes and boosts voltage at the output of the HVBC by connecting a DC/DC module. Figure 1 displays the new wind farm topology, a series-type configuration using HVBC.

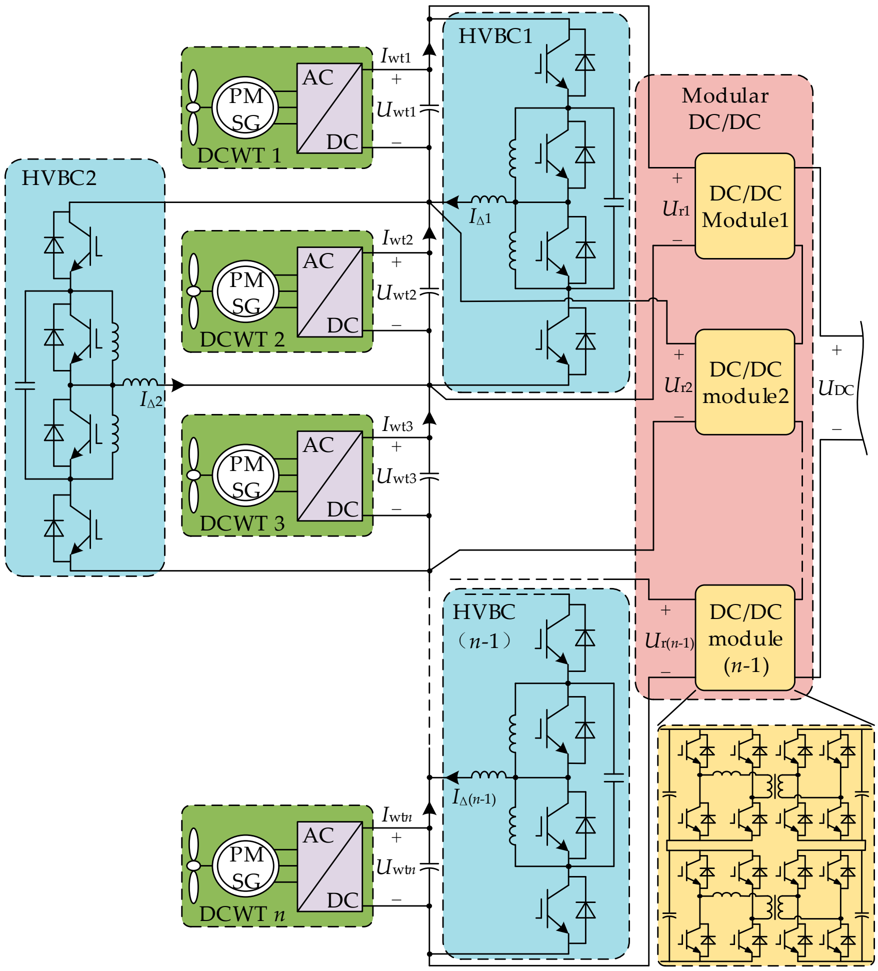

Figure 1. Series-connected all-DC wind farm topology based on HVBC.

As shown in Figure 1, if we consider a series-connected wind farm consisting of n DCWTs, there should be $n-1$ HVBCs. Additionally, the corresponding modular DC/DC system should have $n-1$ DC/DC modules. Each HVBC contains four Insulated Gate Bipolar Transistors (IGBTs) with anti-parallel diodes. The input terminal voltage, U_{ri}, of each DC/DC module is equal to the output terminal voltage of the HVBC connected in parallel with it, which is double the DCWT's U_{wti}. The grid-side inverter controls the output terminal voltage, U_{DC}, of the modular DC/DC converter.

An HVBC is linked in parallel to the output ports of two adjacent DCWTs to convert the voltage change resulting from the difference in wind speed into a change in output current. This is achieved by creating a current pathway for the two surrounding DCWTs. This adjusts the current compensation of the DCWT, ensuring that the current magnitude of each DCWT in the series-connected all-DC wind farm remains unaffected by the other DCWTs when maximum power tracking is attained. This decouples the power in series-connected all-DC wind farms, allowing series-connected wind turbines to attain their highest power production while maintaining balanced voltage conditions. The output of each HVBC is linked in parallel with a DC/DC module, including two dual active bridge (DAB) DC/DC converters [28,29] connected in series. The inputs of each DC/DC module are separate, and the outputs are connected in series to create a novel modular DC/DC system. The modular DC/DC converter primarily ensures voltage equilibrium and voltage amplification at the output of the HVBC while also enhancing fault isolation in all-DC wind farms that are connected in series.

2.2. Principle of Power Decoupling for Series-Connected All-DC Wind Farms Based on HVBC

As an example, Figure 2 illustrates the analysis of the HVBC decoupling concept by considering two DCWTs with identical parameters connected in series.

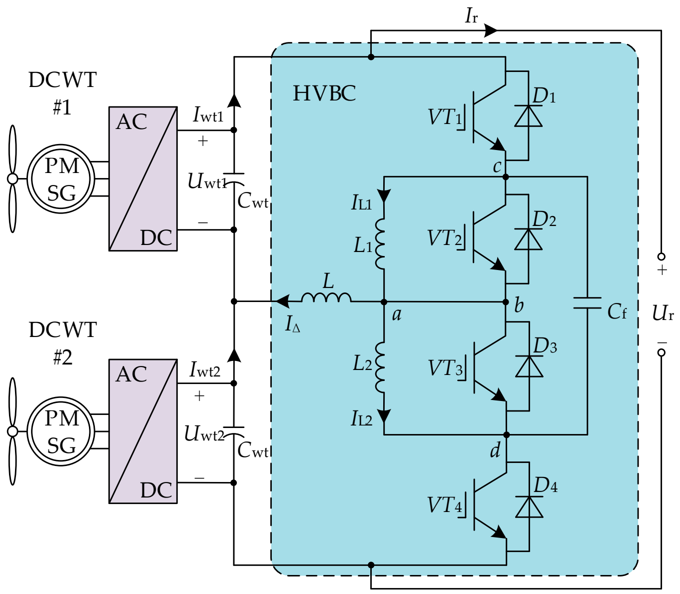

Figure 2. Topology of two DCWTs linked in series based on HVBC.

As per the design requirements, the output terminal voltage of each straight DCWT in a series-type all-DC wind farm should be identical, i.e.,

$$U_{\text{wt1}} = U_{\text{wt2}} = \frac{U_{\text{r}}}{2} = \frac{P_1}{I_{\text{wt1}}} = \frac{P_2}{I_{\text{wt2}}} \tag{3}$$

where U_{r} is the output terminal voltage of the HVBC, and P_1 and P_2 are the output power of DCWT1 and DCWT2, respectively.

The relationship between the output current of the DCWT and the compensating current I_Δ of the HVBC in Figure 2 is determined by the Kirchhoff's Current Law (KCL).

$$I_\Delta = I_{\text{wt1}} - I_{\text{wt2}} \tag{4}$$

The expression for the compensating current I_Δ can be derived from Equations (3) and (4).

$$I_\Delta = \frac{P_1}{U_{\text{wt1}}} - \frac{P_2}{U_{\text{wt2}}} = \frac{1}{U_{\text{r}}/2}(P_1 - P_2) \tag{5}$$

The DC/DC module controls the voltage, U_{r}, at the output of the HVBC, which is assumed to remain constant. In other words, the expression $1/(U_{\text{r}}/2)$ can be represented by a constant value, A. The compensating current I_Δ can be expressed as the power difference ΔP between two adjacent DCWTs:

$$I_\Delta = A(P_1 - P_2) = A \cdot \Delta P \tag{6}$$

Equation (6) demonstrates that the compensation current I_{Δ} is directly proportional to ΔP between two neighboring DCWTs. Therefore, the variation in output power resulting from different wind speeds at the two DCWT locations can be converted into the compensation current value. When there is a disparity in power between two DCWTs, the higher-power DCWT is compensated by the current through the energy storage inductor, L, which maintains a constant ratio of power to current. Currently, the DCWT maintains a steady output voltage to prevent overvoltage. When subjected to the HVBC, each DCWT can produce electricity at its maximum capacity, enhancing the overall power generation efficiency of all-DC wind farms that are connected in series.

Using DCWT1 as a case study, the fluctuation $\Delta U_{\rm wt}$ of the terminal voltage $U_{\rm wt1}$ of the DCWT, induced by the compensating current I_{Δ}, can be mathematically represented as

$$\Delta U_{\rm wt} = \frac{T_{\rm s}^2 U_{\rm wt1}}{C_{\rm wt} L} \tag{7}$$

where T_s is the control period; $C_{\rm wt}$ is the capacitance at the output of the DCWT; and L is the energy-storage inductance of the HVBC. Once the percentage of voltage ripple is established, the value of inductor L can be determined. The following Figure 3 illustrates the effect of different inductance values on the HVBC control performance.

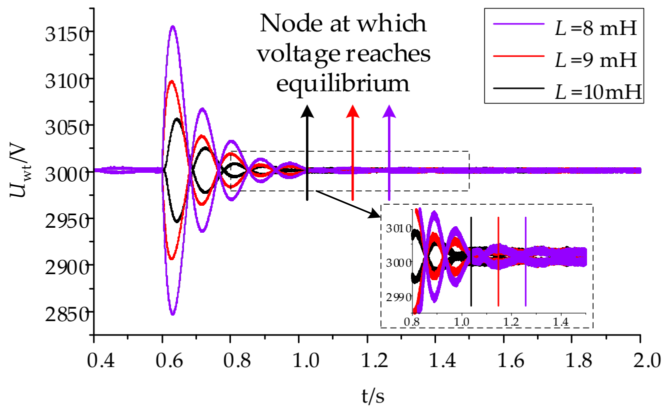

Figure 3. Effect of different inductance values on the control performance of HVBC.

According to the above figure, as the value of L increases, the voltage fluctuation at the ends of the DCWT decreases, and the stabilization time shortens. However, the increased inductance will increase the hardware cost, and the inductor core will occupy a large space. Therefore, the value of L is taken as 10 mH in this study.

3. HVBC's Operating Principle

As depicted in Figure 2, the HVBC comprises four power-switching tubes (VT_1~VT_4, D_1~D_4), two identical freewheeling inductors (L_1 and L_2), an energy storage inductor (L), and a fly-across capacitor ($C_{\rm f}$) connected across the ends of the switching tubes (VT_2 and VT_3). Cf mitigates the voltage shocks experienced by the switching tubes, enhancing the HVBC's stability. Hypothetically, the wind speed is higher at DCWT1 than at DCWT2. In this scenario, the output power of DCWT1, P_1, is greater than the output power of DCWT2, P_2. At this moment, the HVBC supplies a compensating current I_{Δ} to DCWT1, ensuring that the power and current of both DCWTs satisfy the following Equation:

$$\frac{P_1}{(I_{\rm wt1} + |I_{\Delta}|)} = \frac{P_2}{I_{\rm wt2}} = \frac{U_{\rm r}}{2} \tag{8}$$

Conversely, the HVBC supplies I_Δ to DCWT2, ensuring that the requirements are met:

$$\frac{P_1}{I_{\text{wt1}}} = \frac{P_2}{(I_{\text{wt2}} + |I_\Delta|)} = \frac{U_\text{r}}{2} \tag{9}$$

There are three possible scenarios regarding the power difference between two adjacent DCWTs: In the first scenario, P_1 exceeds P_2. L supplies a compensating current to DCWT1, where $I_\Delta > 0$. The second scenario occurs when P_1 is lower than P_2. In this scenario, L supplies a compensating current to DCWT2, where $I_\Delta < 0$. The third scenario occurs when the value of P_1 is equivalent to P_2. In this scenario, L does not supply the compensatory current, where $I_\Delta = 0$. Switching can be achieved by adjusting the carrier phase shift angle, attributable to the opposing directions of the compensation currents in the first two situations. In the third scenario, the two DCWTs can independently balance voltage without involving the HVBC in the regulation process; thus, we have not analyzed this scenario.

The circuit characteristics of the HVBC dictate that switching tubes VT1 and VT4, as well as VT2 and VT3, operate complementarily.

Figure 4 illustrates the waveforms of the four power-switching tubes during operation. The time intervals t_0~t_4 represent one complete operating cycle. The four periods, t_0~t_1, t_1~t_2, t_2~t_3, and t_3~t_4, correspond to the four switching modes of the HVBC power-switching tubes, as indicated in Table 1. The number 0 indicates disconnection, and the number 1 indicates that the tubes are turned on.

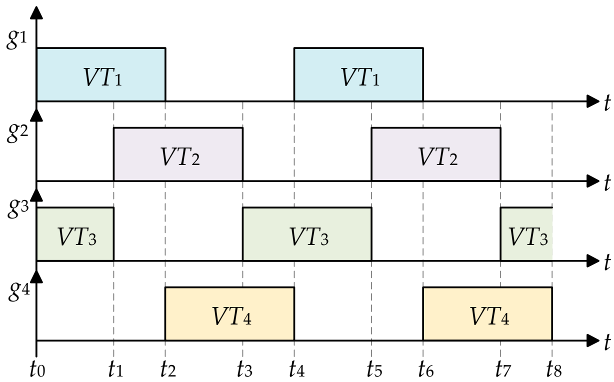

Figure 4. Operating waveform of a power-switching tube.

Table 1. The HVBC switching tubes' operating modes.

Switching Modes and On-Time Periods	Mode 1 t_0~t_1	Mode 2 t_1~t_2	Mode 3 t_2~t_3	Mode 4 t_3~t_4
VT_1	1	1	0	0
VT_2	0	1	1	0
VT_3	1	0	0	1
VT_4	0	0	1	1

Figure 5 illustrates the operational condition of the HVBC during the four switching modes when two nearby DCWTs operate in the first scenario.

In mode 1, VT_1 and VT_3 are active, diverting the current entering the HVBC at node *c*. The diverted current flows through inductor L_1 and capacitor C_f to reach nodes *a* and *d*, respectively. The current passing through inductor L_2 and capacitor C_f combines at node *d* and then travels to node *a* via switching tube VT_3. The compensating current I_Δ is diverted at node *a*, and inductor L_2 is in a state of renewed current. In mode 2, both VT_1 and VT_2 are active, allowing currents to pass through capacitor C_f and inductor L_2. These currents, along with the current passing through switching tube VT_1, converge at node *c*. From there, they flow through inductor L_1 and switching tube VT_2, sequentially, and converge at node a. At node a, I_{Δ} is diverted away. In mode 3, VT_2 and VT_4 are active, allowing the current to pass through diode D_4 and inductor L_2. This current then converges at node d and continues to flow through capacitor C_f toward node c. Next, the electric current passes through inductor L_1 and switching tube VT_2, sequentially, before coming together at node a, where it diverts I_{Δ}. In mode 4, VT_3 and VT_4 conduct, causing the current to flow through diode D_4 and inductor L_2. This current converges at node d and then passes through diode D_3, capacitor C_f, and inductor L_1, converging at node a. At node a, I_{Δ} is diverted, while inductor L_2 enters a state of renewed current.

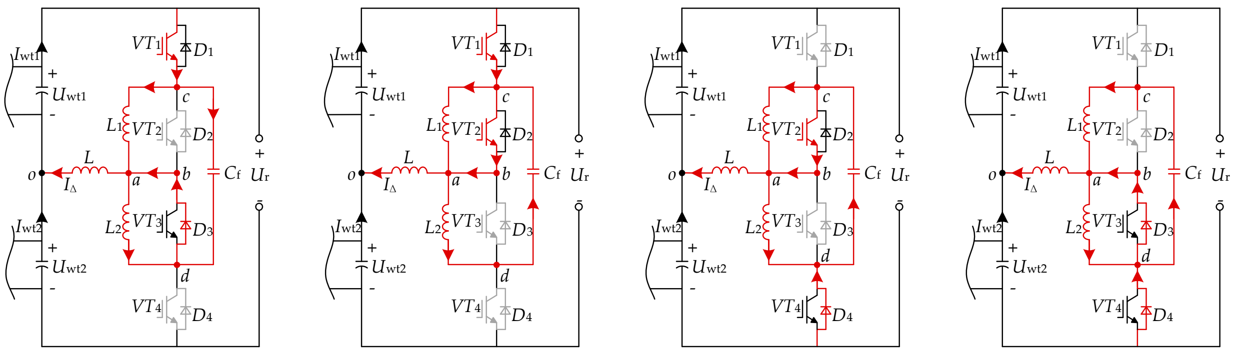

(**a**) Mode 1 (**b**) Mode 2 (**c**) Mode 3 (**d**) Mode 4

Figure 5. The operating state of HVBC in the first scenario. (**a**) Operating status of mode 1; (**b**) operating status of mode 2; (**c**) operating status of mode 3; (**d**) operating status of mode 4.

Figure 6 illustrates the operational states of the HVBC during the four switching modes when two nearby DCWTs operate in the second scenario.

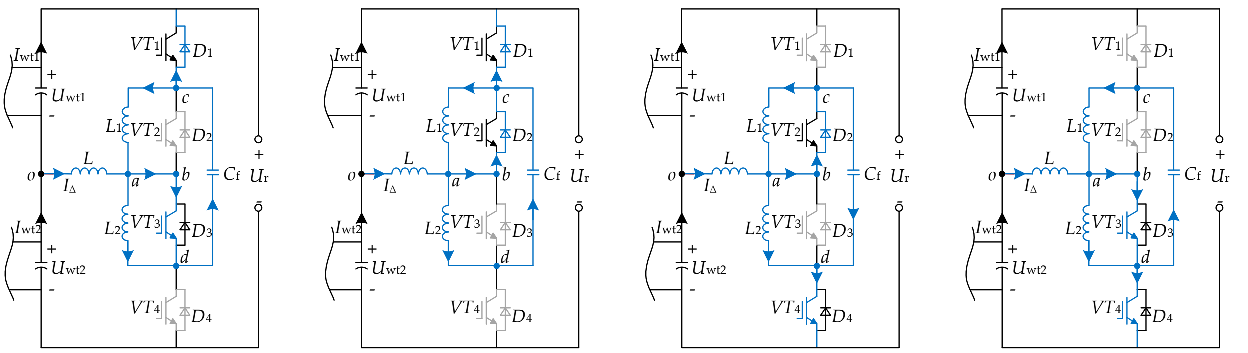

(**a**) Mode 1 (**b**) Mode 2 (**c**) Mode 3 (**d**) Mode 4

Figure 6. The operating state of HVBC in the second scenario. (**a**) Operating status of mode 1; (**b**) operating status of mode 2; (**c**) operating status of mode 3; (**d**) operating status of mode 4.

When two neighboring DCWTs operate in the second scenario, the current flow in the HVBC can be compared with the first scenario and, thus, will not be reiterated.

Under the HVBC's action, the output terminal voltages of each DCWT in a series-connected all-DC wind farm are identical. Considering two DCWTs connected in series, as seen in Figure 2, the cumulative power generated by the wind farm can be calculated as follows:

$$P_{\sum} = P_1 + P_2 = I_r U_r \tag{10}$$

The output power of the two DCWTs is represented as

$$\begin{cases} P_1 = I_{wt1} U_{wt1} = I_{wt1} \frac{U_r}{2} \\ P_2 = I_{wt2} U_{wt2} = I_{wt2} \frac{U_r}{2} \end{cases} \tag{11}$$

The output current of the series cluster, I_r, created by the two DCWTs linked in series can be calculated using Equations (10) and (11).

$$I_r = \frac{I_{wt1} + I_{wt2}}{2} \tag{12}$$

The above equation can be expanded to a series cluster of n DCWTs. When n DCWTs are connected in series, the DC I_{rs} output from the series cluster can be expressed as

$$I_{rs} = \frac{I_{wt1} + I_{wt2} + \cdots + I_{wtn}}{n} = \frac{1}{n}\sum_{i=1}^{n} I_{wti} \tag{13}$$

Then, the output power of the series-type all-DC wind farm is

$$P_{\sum} = (\frac{1}{n}\sum_{i=1}^{n} I_{wti})U_{rs} = \frac{U_{rs}}{n}\sum_{i=1}^{n} I_{wti} = \sum_{i=1}^{n} P_i \tag{14}$$

where U_{rs} is the output voltage of a series cluster consisting of n DCWTs connected in series.

Equation (14) demonstrates that when the series-type all-DC wind farm is connected to the HVBC, each DCWT can achieve maximum power output. The total power output of the wind farm is the sum of the output power of each DCWT, resulting in improved power generation efficiency.

4. Control Strategy Based on HVBC for Series-Connected All-DC Wind Farms

Figure 7 illustrates a comprehensive control method for an HVBC-based series-type all-DC wind farm.

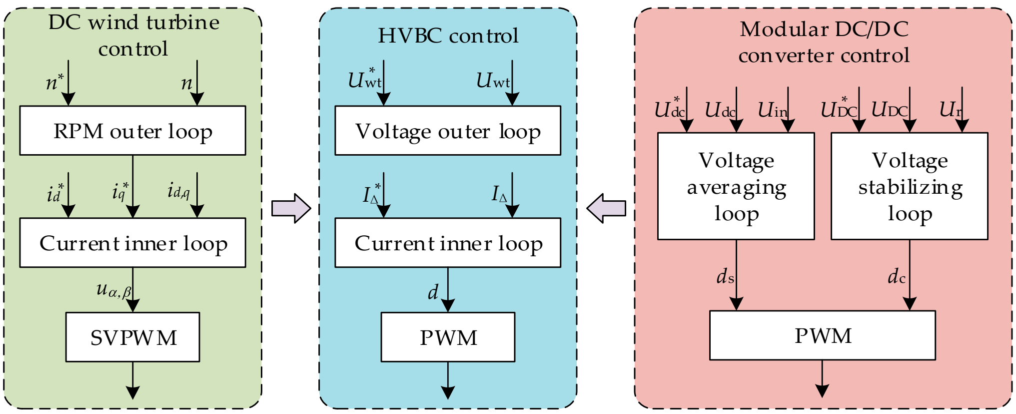

Figure 7. Overall control strategy for series-connected all-DC wind farms based on HVBC.

The overall control method for wind farms consists of three components: DCWT control, HVBC control, and modular DC/DC converter control. The functions to be achieved include voltage equalization the control of a series-connected DCWT using an HVBC under varying wind speeds; the active power control of the DCWT output; the maximum wind energy tracking control of the permanent magnet synchronous generator (PMSG); and implementing a modular DC/DC converter to control voltage stabilization at the input end and voltage equalization at the output end. Using a machine-side AC/DC converter allows the PMSG to achieve maximum wind energy tracking control and manage the active power output of the DCWT. The HVBC equalizes the output voltage of the series-connected DCWTs using a double closed-loop regulation system that controls the voltage outer loop and the current inner loop. The DAB-based modular DC/DC converter ensures that the voltage is equalized at the output of each DC/DC module and stabilizes the voltage at the output of the HVBC by stabilizing U_{ri}.

4.1. HVBC's Control Strategy

The HVBC decouples the power–current in series-type all-DC wind farms by supplying a compensation current to maintain voltage balance in the series-connected DCWTs. As the DC/DC converter regulates the voltage at the HVBC's output, control must be applied to the output voltage of only one DCWT in each HVBC. The control object in the HVBC is the output terminal voltage U_{wt} of a DCWT. When U_{wt} exceeds the reference voltage U_{wt}*, the HVBC injects a compensating current into the series-type all-DC wind farm through L. Conversely, if the U_{wt} value of the DCWT is lower than U_{wt}*, the HVBC will extract a compensating current from the series-connected all-DC wind farm through L. The HVBC can be regulated using a closed-loop control approach, which comprises a voltage outer loop and a current inner loop. Thus, the optimal control approach for an HVBC should be a dual closed-loop system comprising an outer loop for voltage control and an inner loop for current control. This HVBC control strategy is depicted in Figure 8.

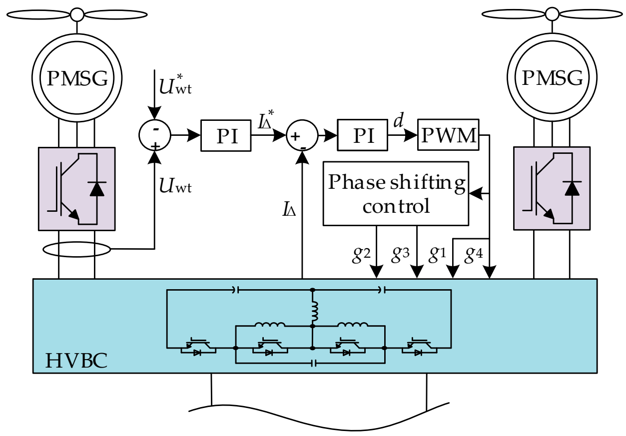

Figure 8. HVBC's control strategy.

The discrepancy between the machine-end voltage U_{wt} of the DCWT and U_{wt}* is transmitted through the outer-loop PI controller to derive the reference value I^*_Δ of the compensation current. The disparity between the compensation currents I_Δ and I^*_Δ is then transmitted through the inner-loop PI controller to obtain the duty cycle signal, d. The drive signal of the HVBC is acquired using PWM modulation.

The expressions for the voltage outer loop, PI_1, and the current inner loop, PI_2, are shown in Equation (15). The control block diagram of the HVBC, depicted in Figure 8, can be drawn as per Figure 9.

$$\begin{cases} PI_1 = \frac{sK_{p1}+K_{i1}}{s} \\ PI_2 = \frac{sK_{p2}+K_{i2}}{s} \end{cases} \quad (15)$$

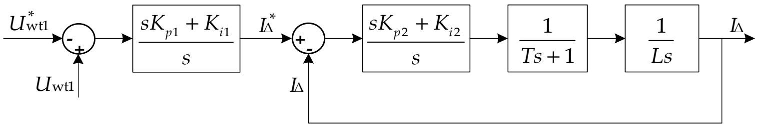

Figure 9. Control diagram of HVBC.

The error between the actual and given voltage values at both ends of the DCWT passes through the PI controller to obtain the reference value of the compensation current, as shown in the following equation.

$$I^*_\Delta = (U_{wt1} - U^*_{wt2}) \cdot \frac{sK_{p1}+K_{i1}}{s} \quad (16)$$

Using Mason's formula, the closed-loop transfer function of the HVBC control block diagram can be obtained, as shown in Equation (17).

$$\Phi(s) = \frac{I_\Delta(s)}{I_\Delta^*(s)} = \frac{K_{p2}s + K_{i2}}{TLs^3 + Ls^2 + K_{p2}s + K_{i2}} \tag{17}$$

According to the Laws criterion, the conditions shown in Equation (18) need to be satisfied to ensure that the system is stabilized.

$$K_{i2} < \frac{1}{T}K_{p2} \tag{18}$$

Taking the HVBC operating mode shown in Figure 5a as an example, the relationship between the power difference between two DCWTs and d can be analyzed. According to Kirchhoff's Voltage Law (KVL),

$$U_\mathrm{L} + U_\mathrm{L1} = L\frac{\mathrm{d}i_\Delta}{\mathrm{d}t} + L_1\frac{\mathrm{d}i_\mathrm{L1}}{\mathrm{d}t} = U_\mathrm{wt1} \tag{19}$$

$$U_{C_\mathrm{f}} = U_\mathrm{L1} \tag{20}$$

Joining the above two equations, the electric current passing through the fly-across capacitance C_f can be expressed as

$$I_{C_\mathrm{f}} = C_\mathrm{f}\frac{\mathrm{d}u_{C_\mathrm{f}}}{\mathrm{d}t} = C_\mathrm{f}L_1(\mathrm{d}\frac{\mathrm{d}i_\mathrm{L1}}{\mathrm{d}t}/\mathrm{d}t) \tag{21}$$

The preceding equation can be integrated to obtain the following result:

$$I_{C_\mathrm{f}} \cdot (dT)^2 = C_\mathrm{f}L_1 \cdot I_\mathrm{L1} \tag{22}$$

This is obtained via generalized nodal analysis:

$$I_{VT_1} = I_\mathrm{L1} + I_{C_\mathrm{f}} = I_\Delta \tag{23}$$

From Equations (22) and (23), the relationship between I_L1 and I_Δ can be expressed as

$$I_\mathrm{L1} = \frac{(dT)^2}{C_\mathrm{f}L_1 + (dT)^2}I_\Delta \tag{24}$$

The preceding Equation can be integrated to obtain

$$U_\mathrm{wt1} \cdot dT = L \cdot I_\Delta + L_1 I_\mathrm{L1} \tag{25}$$

Per Equations (6), (24), and (25), the relationship between the ΔP and d values of two neighboring DCWTs can be derived as

$$\Delta P = \frac{(dT)^3 + C_\mathrm{f}L_1 dT}{(L + L_1)(dT)^2 + C_\mathrm{f}LL_1} \cdot \frac{U_\mathrm{wt1}U_\mathrm{r}}{2} \tag{26}$$

The Equation above has a strictly increasing trend when d is within the interval [0, 1], attaining its maximum value when $d = 1$. By appropriately adjusting the parameters of the HVBC, it is possible to increase the power difference between two adjacent DCWTs beyond the rated power of a single DCWT. Thus, in the event of failure, if one of the DCWTs is disconnected, it can still maintain the efficient functioning of the series-connected DC wind farm. Furthermore, the wind farm's stability increases as more DCWTs are connected in series, enabling more DCWTs to be disconnected without affecting operations.

4.2. DCWT's Control Strategy

Figure 10 illustrates the DCWT control strategy [30].

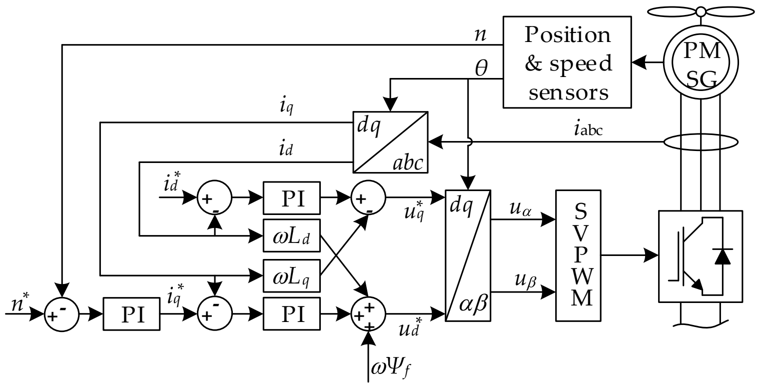

Figure 10. DCWT's control strategy.

The reference value for rotational speed, denoted by n^*, is determined using the optimal tip speed ratio control method. After n^* is compared with the rotational speed n detected by the speed sensor, the reference value for the q-axis current, i_q^*, can be obtained through PI regulation. The reference value for the d-axis current, i_d^*, is set to zero. The values i_q^* and i_d^* are obtained through coordinate transformation. These values represent the difference between the current inner loop decoupling controls. The generator stator d-axis and q-axis voltage reference values u_d^* and u_q^* are obtained after the dq-$\alpha\beta$ coordinate transformation. The voltage values u_α and u_β are obtained in the $\alpha\beta$ coordinate system after the transformation. Finally, the control signal of the machine side rectifier is obtained through SVPWM modulation. The PMSG's active power regulation is achieved by monitoring the stator voltage reference value and adjusting it based on the three-phase voltage value of the PMSG stator output. This allows the PMSG to optimally track the maximum wind energy.

4.3. Control Strategy for Modular DC/DC Converters

Figure 11 depicts the control method, assuming that the modular DC/DC converter comprises m DAB modules in total.

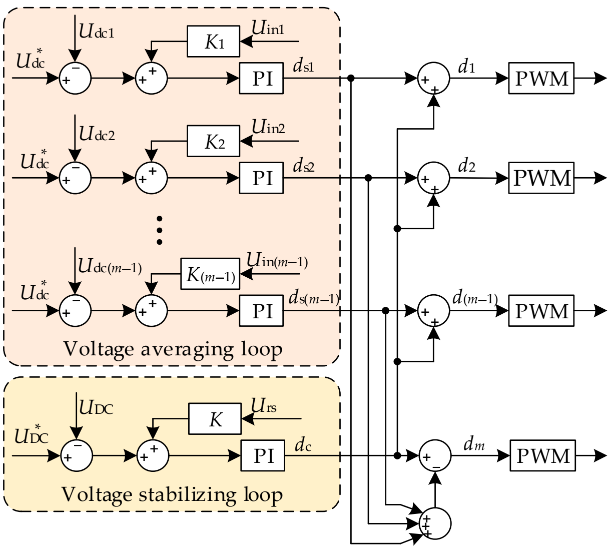

Figure 11. Control strategy for modular DC/DC converters.

As a sub-module of the modular DC/DC converter, a dual active bridge isolation converter is utilized in considering the DCWT startup procedure and the isolation requirements. Equalizing each module's output voltage and maintaining a steady input voltage are the control goals of the modular DC/DC converter. Owing to the variations in each module's specifications, an imbalanced voltage output will result from each module's control strategy adopting the same shift ratio. This will immediately impact the modular DC/DC converter's stability. Therefore, equalization control must be added to each DAB module, and each DAB module's shift ratio can be acquired by correcting this ratio [31,32].

As illustrated in Figure 11, $U_{\mathrm{in}i}$ and $U_{\mathrm{dc}i}$ stand for the input and output voltage values of the i th DAB module, respectively; $U_{\mathrm{DC}}{}^{*}$ represents the wind farm's output voltage reference; U_{DC} represents the wind farm's actual output voltage; and U_{rs} represents the HVBC's total voltage value. The shift ratio d_i of the i th DAB module can be obtained by adding the modified shift ratio $d_{\mathrm{s}i}$ from the voltage equalization link to the common shift ratio d_{c} from the voltage stabilization link. PWM modulation is then used to extract the control signal from the switching tube of the DAB module.

4.4. Control Flowchart of HVBC-Based Series-Type All-DC Wind Farm

Taking two DCWTs in series in Figure 2 as an example, the wind speeds of the two DCWTs can be denoted as $v_{\mathrm{w}1}$ and $v_{\mathrm{w}2}$, and the active power emitted can be denoted as P_1 and P_2. The remaining quantities are labeled in Figure 2. The voltages of the two DCWTs are assumed to be equal under the initial conditions, i.e., $U_{\mathrm{wt}1} = U_{\mathrm{wt}2}$. The control flowchart of the HVBC-based series-connected all-DC wind farm is shown in Figure 12 when the wind speed varies.

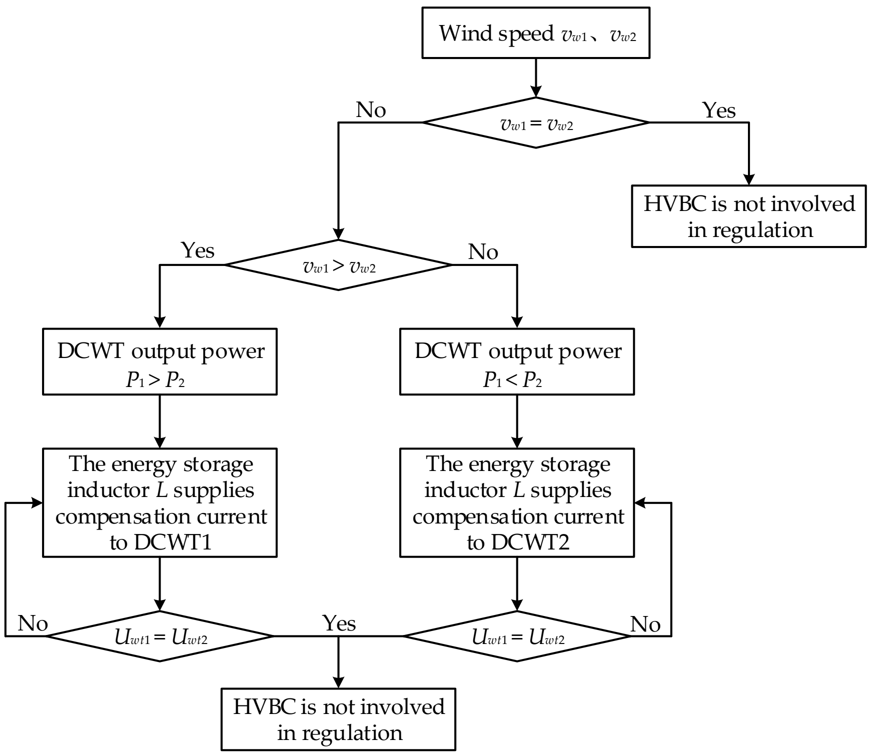

Figure 12. Control flowchart of HVBC-based series-type all-DC wind farms.

5. Simulation Verification

This study constructed a 60 kV/48 MW series-type all-DC wind farm model using the Matlab-2022b/Simulink simulation platform to confirm the viability and efficacy of the designed HVBC. The model is shown in Figure 13. Table 2 displays the primary design parameters.

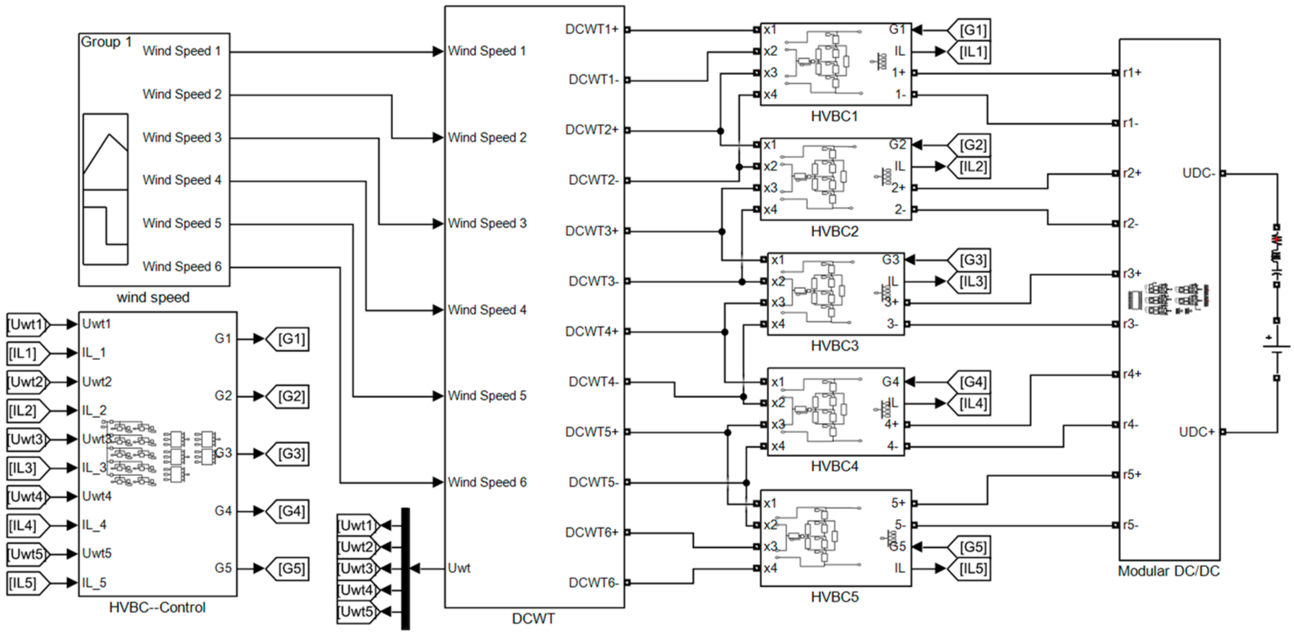

Figure 13. Simulink modeling of a 60 kV/48 MW series-type all-DC wind farm based on HVBC.

Table 2. Design parameters of HVBC-based series-type all-DC wind farms.

Parts	Parameters	Value
Wind farm	Number of DCWT n	6
	Rated capacity of wind farm S (MW)	48
	DC transmission voltage U_{DC} (kV)	60
	Rated wind speed v_w (m/s)	12
DCWT	Stand-alone capacity S_{wt} (MW)	8
	Rated output voltage U_{wt} (kV)	3
HVBC	Energy-storage inductor L (mH)	10
	Freewheeling inductors L_1, L_2 (mH)	1
	Fly-across capacitor C_f (mF)	30
	Switching frequency f_{sw} (kHz)	10
Modular DC/DC converter	Number of single modules m	5
	Number of DAB modules in a single module x	2
	Single module output voltage U_{dc} (kV)	12

Excluding the measurement module, our Simulink consists of five main modules, i.e., the module for generating wind speed, the module for a series wind farm consisting of six DCWTs, the module for the HVBC, the control module for the HVBC, and the module for the modular DC/DC converter.

This simulation primarily validates the stability of the designed wind farm in the presence of uneven wind speeds, abrupt changes in wind speeds, and wind turbine failure shutdown situations. This research establishes a comparative simulation to emphasize the stabilizing impact of HVBCs on the output voltage of in-series DCWTs.

5.1. Comparison Simulation

To demonstrate the effectiveness of the HVBC, we simulate a hypothetical scenario of wind speed variations at a wind farm. It is hypothesized that at 0.8 s, the wind speed at each DCWT location transitions from the reported wind speed to the following speeds: 13 m/s, 12 m/s, 11 m/s, 10 m/s, 9 m/s, and 8 m/s.

The simulated waveforms of each DCWT's output voltage in a conventional series-connected all-DC wind farm are shown in Figure 14a. Figure 14b shows the output current of the series cluster consisting of DCWTs coupled in a series configuration.

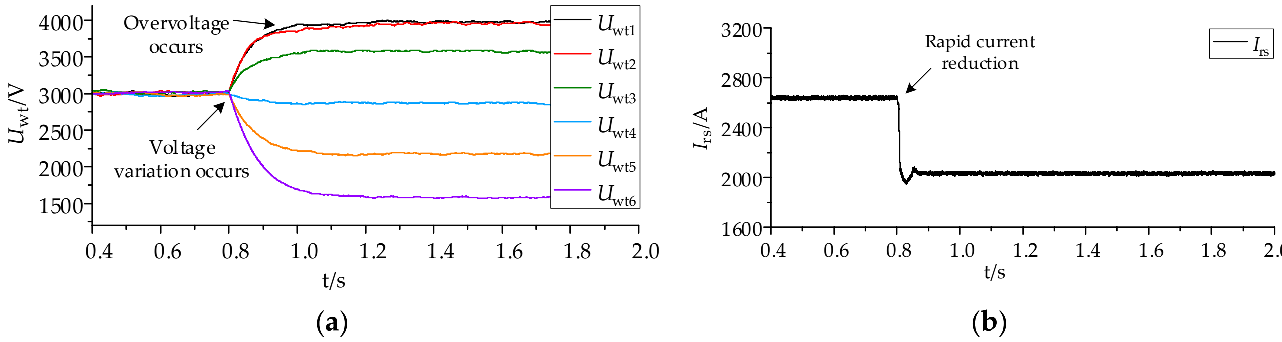

Figure 14. Simulation of a conventional series-type all-DC wind farm. (**a**) Output voltage of DCWTs; (**b**) output current of series clusters.

According to the simulated waveforms shown in Figure 14, the output voltage of the wind farm remains constant. This is due to the control exerted by the grid-connected inverter. At 0.8 s, the wind speed of the entire wind farm declines, reducing the electricity generated. Consequently, the output current of the series cluster is reduced from 2667 A to 2040 A. When the output current of a series cluster falls, the output voltage of some of the DCWTs in the cluster suddenly increases. This leads to a maximum overvoltage of approximately 1 kV, significantly impacting the safe and stable functioning of the wind farm.

Figure 15 shows the simulated waveforms of the output voltage of each DCWT in a series-connected all-DC wind farm under the influence of an HVBC.

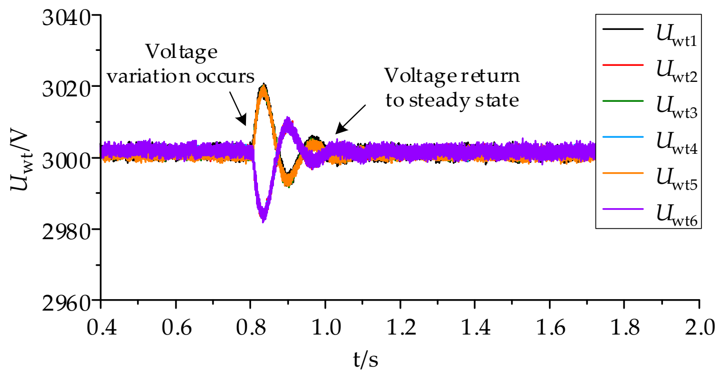

Figure 15. Simulation of HVBC-based series-type all-DC wind farms.

According to the simulated waveforms, the wind speed suddenly changes at 0.8 s. Currently, owing to the influence of the HVBC, the output voltage of each DCWT in the wind farm experiences minor turbulence and then rapidly settles at approximately 3 kV. The HVBC mitigates the potential for overvoltage caused by abrupt changes in wind speed in certain wind turbines inside the all-DC wind farm, enhancing its safety and stability.

5.2. Operating with Unequal Wind Speeds

The wind speed at each DCWT location is assumed to be consistently maintained at 14 m/s, 13 m/s, 12 m/s, 11 m/s, 10 m/s, and 9 m/s. Given that the wind speeds at DCWT1 to DCWT3 are equal to or higher than the rated wind speeds they are designed for, the first three DCWTs are generating power at their rated capacity. Theoretical estimates for the output power of the remaining DCWTs are 7.2 MW, 5.8 MW, and 4.4 MW. Figure 16 shows the simulated waveforms for operations under varying wind speed conditions.

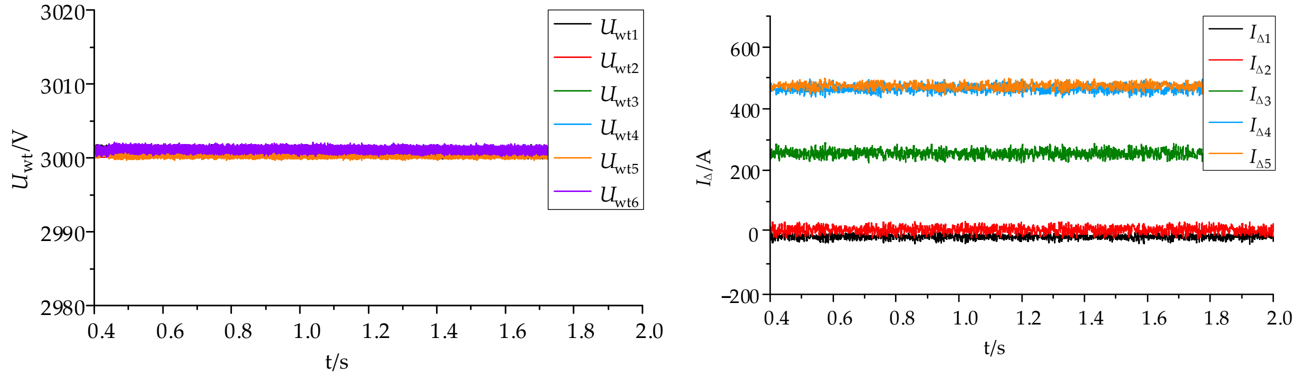

(**a**) Output voltage of DCWTs (**b**) Compensation current provided by HVBCs

Figure 16. Operating with unequal wind speeds. (**a**) Simulated waveforms of each DCWT output voltage; (**b**) simulated waveforms of HVBC supplying compensation current to series DCWT.

Figure 16a demonstrates that the HVBC system can stabilize each DCWT's output voltage at about 3 kV, confirming that the HVBC proposed in this study effectively stabilizes the voltage of series-connected DCWTs in the presence of unequal wind speeds.

According to Figure 16b, the power differential can be estimated to be zero because DCWTs 1, 2, and 3 all function at their rated state. Consequently, the compensating currents $I_{\Delta1}$ and $I_{\Delta2}$ provided by the first two HVBCs can be maintained at a stable value close to 0. The power disparity between DCWT3 and DCWT4 is 0.8 MW. Based on Equation (5), it can be inferred that the compensation current $I_{\Delta3}$ is 267 A. The simulation results depicted in Figure 16b exhibit a high degree of proximity to the corresponding theoretical values. Furthermore, the compensation current $I_{\Delta4}$ generated by the fourth HVBC is nearly equivalent to the compensation current $I_{\Delta5}$ produced by the fifth HVBC, owing to the comparable power discrepancy between DCWTs 4 and 5, as well as between DCWTs 5 and 6. Examining the relationship between the output power of each DCWT and the compensation current confirms that the amount of compensation current is directly proportional to the ΔP value between the outputs of two adjacent DCWTs.

5.3. Operating during Rapid Changes in Wind Speed

Wind speed variations at six DCWTs in a hypothetical series-type all-DC wind farm are shown in Figure 17.

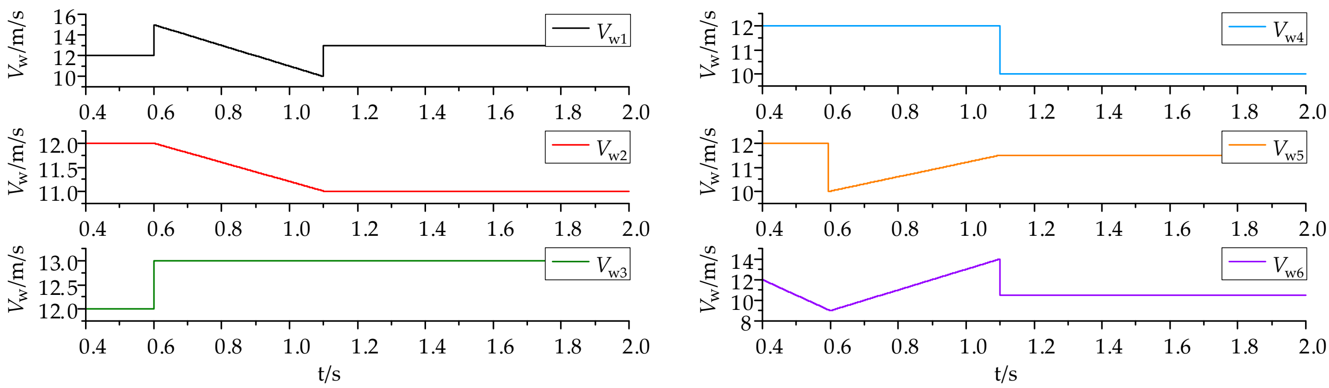

Figure 17. Rapid changes in wind speed in series-connected all-DC wind farms.

The wind speeds at the six DCWTs change within a time frame of 0.6 s to 1.1 s. After 1.1 s, the wind speeds at the specific positions of DCWT1 to DCWT6 reach a stable state, measuring 13 m/s, 11 m/s, 13 m/s, 10 m/s, 11.5 m/s, and 10.5 m/s, respectively. The operation during rapid wind speed change conditions is shown in Figure 18.

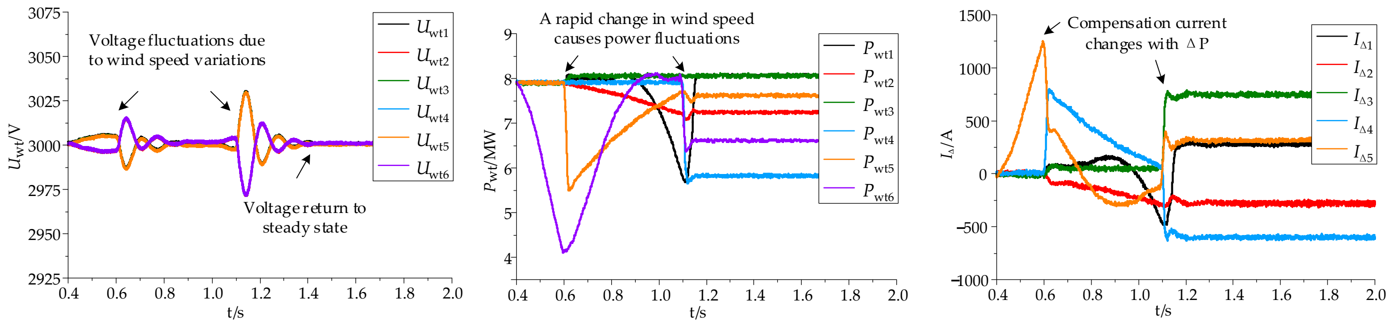

(**a**) Output voltage of DCWTs (**b**) Output power of DCWTs (**c**) Compensation current provided by HVBCs

Figure 18. Operation under conditions of rapid changes in wind speed. (**a**) Simulated waveforms of each DCWT output voltage; (**b**) simulated waveforms of each DCWT output power; (**c**) simulated waveform of compensation current supplied by HVBC to series DCWTs.

Figure 18a demonstrates that when there is a fast shift in wind speed in a series-connected all-DC wind farm, the output voltage of each DCWT fluctuates. However, the output terminal voltage of the DCWTs immediately stabilizes at around 3 kV, owing to the HVBC's influence. This confirms that the HVBC suggested in this study effectively stabilizes the voltage of a series-connected DCWT in an all-DC wind farm when there are rapid wind speed variations.

Figure 18b demonstrates that the output power of each DCWT can precisely and effectively adjust to wind speed variations. The wind farm's DCWTs can achieve maximum power output even when there are wind speed changes. This confirms that the HVBC can successfully decouple the power of all series-connected all-DC wind farms and effectively enhance their power generation efficiency.

Figure 18c shows that the amplitude of the compensating current is directly proportional to the power differential between two adjacent DCWTs. If the power differential between two adjacent DCWTs is positive, then the compensation current provided by the HVBC to the series-connected DCWTs is also positive. If the power difference between two adjacent DCWTs is negative, the compensation current's amplitude is also negative. This indicates that the HVBC draws the compensation current from the in-series DCWTs.

5.4. Operating with Wind Turbine Failure Shutdown

When a DCWT of a wind farm malfunctions or undergoes repair, it is necessary to deactivate the DCWT. Imagine that, one second ago, each DCWT was operating at its rated state, and after one second, DCWT2 was taken out of operation, owing to a fault. Currently, DCWT2 produces no output power, while the other DCWTs continue to output power at their rated levels. The simulated waveforms of the output voltage of each DCWT in the wind farm are depicted in Figure 19.

The simulation results in the above figure show that when one DCWT in the series-connected all-DC wind farm is shut down, the output terminal voltage of each remaining DCWT fluctuates, but it soon stabilizes at about 3 kV. In addition, the voltages at the ends of the capacitors connected to DCWT2 are clamped by the HVBC at about 3 kV.

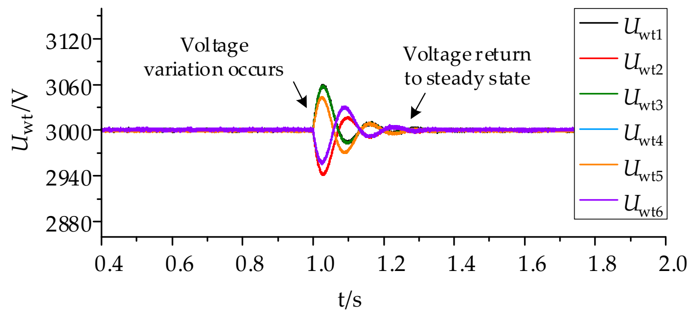

Figure 19. The operation of each DCWT in a wind farm when one DCWT is shut down.

At 1 s, DCWT2 and DCWT4 are deactivated because of a malfunction. When DCWT2 and DCWT4 are deactivated, their output power decreases to zero, while the output power of the remaining DCWTs remains unaffected. Figure 20 shows the simulated waveforms of the output voltage for each DCWT in the wind farm.

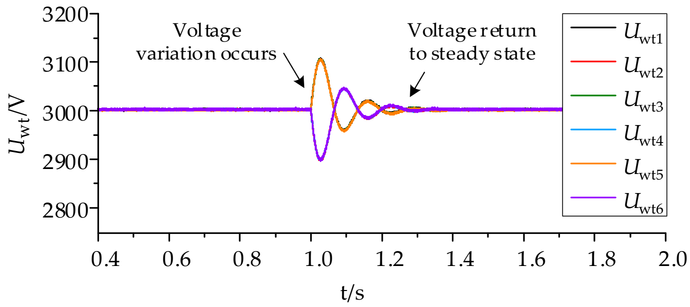

Figure 20. The operation of each DCWT in a wind farm when two DCWTs are shut down.

The simulation results in the Figure above show that when two DCWTs in a series-connected all-DC wind farm are deactivated, the output terminal voltage of each remaining DCWT fluctuates momentarily but rapidly stabilizes at approximately 3 kV. Additionally, the voltages at both terminals of the capacitors connected to DCWT2 and DCWT4 are regulated by the HVBC at around 3 kV. Comparing Figure 19 with Figure 20 shows that as the number of DCWTs in the wind farm cut-out operation increases, the voltage fluctuation at both ends of the DCWT at the moment of cut-out also increases. This is caused by an increase in the total power difference between the neighboring DCWTs.

Figure 21 shows simulated waveforms of the output voltage and output power of each DCWT in the wind farm when DCWTs 2, 3, and 4 are simultaneously deactivated after 1 s.

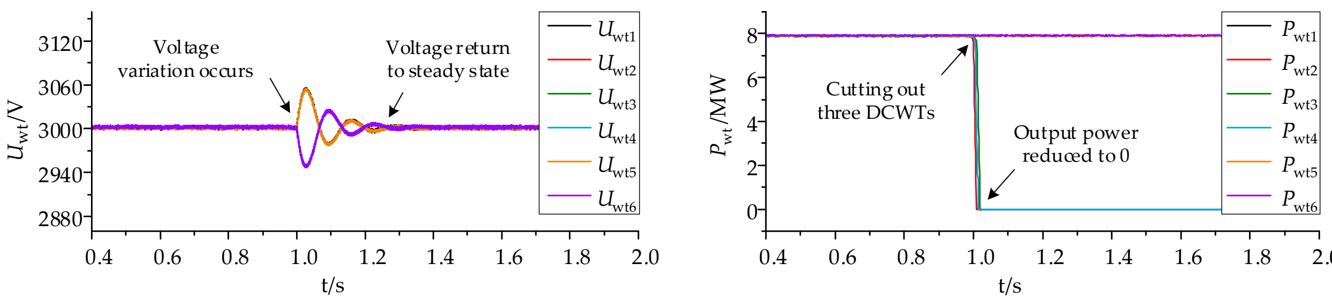

(**a**) Output voltage of DCWTs (**b**) Output power of DCWTs

Figure 21. The operation of each DCWT in a wind farm when three DCWTs are shut down. (**a**) Simulated waveforms of each DCWT output voltage; (**b**) simulated waveforms of each DCWT output power.

Based on the modeled findings depicted in the Figure above, it can be inferred the HVBC effectively limits the voltage at the terminals of the capacitors linked to DCWTs 2, 3, and 4 to approximately 3 kV. After removing DCWTs 2, 3, and 4 from operation, their power output decreases to zero. However, the remaining DCWT continues to output power at the rated level. This confirms that the HVBC effectively decouples power and ensures that the remaining DCWTs are unaffected by removing the others. The DCWT can effectively maintain a stable output voltage throughout the cutover operation, enhancing the stability and reliability of the wind farm. When comparing Figure 20 with Figure 21a, we can see that although the number of DCWTs taken out of operation increases, the voltage fluctuation of each at the moment of cut-out decreases. This is because the total power difference between neighboring DCWTs decreases.

6. Conclusions

This study proposed an HVBC topology and control strategy applicable to large-capacity series-connected all-DC wind farms. We did so to adapt to the large-capacity and large-scale development of new energy sites represented by wind energy. This research can help full-DC wind farms realize safer and more reliable operations, help construct new large-scale energy bases, and promote the transition of global energy to renewable energy.

To maintain voltage balance between the output terminals of each DCWT in a series-connected all-DC wind farm, enhance operational stability, and prevent a decrease in power generation efficiency due to the addition of voltage-limiting settings, this study introduced a novel circuit topology called a half-bridge voltage balancing circuit, designed for use in series-connected all-DC wind farms. First, the operational mechanism of the HVBC was examined, and then a control method was designed to ensure that the output voltage of each DCWT is balanced while the farm works under various conditions. Finally, the viability of the HVBC topology was confirmed via simulation. The conclusions are as follows:

1. The suggested HVBC design efficiently decouples power in a DCWT series, ensures balanced output voltage across each DCWT, and mitigates the risk of overvoltage in the DCWT series caused by wind speed variations.
2. After the HVBC is connected to the series-connected all-DC wind farm, each DCWT can realize its maximum power output under output voltage balance conditions. This enhances the overall power generation efficiency of the wind farm.
3. When a section of the DCWTs in a series-connected all-DC wind farm is taken out of operation owing to a fault or for maintenance purposes, the HVBC can limit the capacitive voltage at the DCWT output to its normal operating value. This enhances the stability and dependability of the wind farm's operations.

The HVBC topology proposed in this paper has good application prospects for series-type all-DC wind farms. Further research can be conducted by considering two perspectives: first, research on applying HVBCs to offshore all-DC wind farms with higher voltage levels, and second, in-series–parallel-type all-DC wind farms can be considered to adapt to the development of large-scale and large-capacity offshore all-DC wind farms.

Author Contributions: Conceptualization, Z.L.; methodology, X.S.; software, X.S.; validation, X.S.; formal analysis, X.S.; investigation, X.S.; writing—original draft preparation, X.S.; writing—review and editing, Q.M.; supervision, H.W.; project administration, H.W.; funding acquisition, H.W. All authors have read and agreed to the published version of the manuscript.

Funding: This research was funded by the National Key Research and Development Program of China, grant number 2021YFB1507005.

Data Availability Statement: Data are contained within the article.

Conflicts of Interest: Author Zhanlong Li was employed by the company Beijing Goldwind Science & Creation Wind Power Equipment Co., Ltd. The remaining authors declare that the research was conducted in the absence of any commercial or financial relationships that could be construed as potential conflicts of interest.

References

1. Bilgili, M.; Yasar, A.; Simsek, E. Offshore wind power development in Europe and its comparison with onshore counterpart. *Renew. Sust. Energ. Rev.* **2011**, *15*, 905–915. [CrossRef]
2. Rodrigues, S.; Restrepo, C.; Kontos, E.; Teixeira Pinto, R.; Bauer, P. Trends of offshore wind projects. *Renew. Sust. Energ. Rev.* **2015**, *49*, 1114–1135. [CrossRef]
3. Su, X.; Wang, X.; Xu, W.; Yuan, L.; Xiong, C.; Chen, J. Offshore Wind Power: Progress of the Edge Tool, Which Can Promote Sustainable Energy Development. *Sustainability* **2024**, *16*, 7810. [CrossRef]
4. GWEC. Global Wind Report 2024. Available online: https://gwec.net/global-wind-report-2024/ (accessed on 16 April 2024).
5. Xu, C.; Jiao, Z.; Han, X.; Huang, Y.; Wang, J.; Zhang, H.; Shen, W. Comprehensive layout optimization of the transmission system in a deepwater wind farm cluster. *Front. Energy Res.* **2023**, *11*, 1268291. [CrossRef]
6. Yang, B.; Liu, B.; Zhou, H.; Wang, J.; Yao, W.; Wu, S.; Shu, H.; Ren, Y. A critical survey of technologies of large offshore wind farm integration: Summary, advances, and perspectives. *Prot. Control Mod. Power Syst.* **2022**, *7*, 17. [CrossRef]
7. Song, Y.; Chang, X.; Wang, H. Comprehensive Evaluation Model and Methodology for Offshore Wind Farm Collection and Transmission Systems. *J. Mar. Sci. Eng.* **2023**, *11*, 2169. [CrossRef]
8. Veilleux, E.; Lehn, P. Interconnection of Direct-Drive Wind Turbines Using a Series-Connected DC Grid. *IEEE Trans. Sustain. Energy* **2014**, *5*, 139–147. [CrossRef]
9. Kong, Q.; Song, G.; LI, Z.; Wang, X. Design of a Series–Parallel All-DC Power Generation System Based on a New DC Wind Turbine. *Electronics* **2023**, *12*, 2967. [CrossRef]
10. Han, H.; Li, Z.; Wang, H.; Feng, Q.; Guo, R.; Yang, Z.; Liu, X. Design of a Parallel All-DC Wind Power System with Turbine-Side Boost Based on a New DC Conversion. *IEEE Access* **2024**, *12*, 3054–3069. [CrossRef]
11. Almeida, A.; Almeida, P.; Barbosa, P. Design Methodology for the DC Link Current Controller of a Series-Connected Offshore Wind Farm with a Droop Control Strategy. *IEEE Trans. Ind. Appl.* **2024**, *60*, 3568–3577. [CrossRef]
12. Xie, L.; Cheng, F.; Wu, J. Control Strategy for Offshore Wind Farms with DC Collection System Based on Series-Connected Diode Rectifier. *Sustainability* **2022**, *14*, 7860. [CrossRef]
13. Verma, N.; Kumar, N. DFIG-Based Wind Plant Coupled Series Compensated Transmission Line: Modeling and SSR Stability Analysis. *J. Inst. Eng. India Ser. B* **2022**, *103*, 1917–1926. [CrossRef]
14. Zhang, H.; Gruson, F.; Rodriguez, D.; Saudemont, C. Overvoltage Limitation Method of an Offshore Wind Farm with DC Series-Parallel Collection Grid. *IEEE Trans. Sustain. Energy* **2019**, *10*, 204–213. [CrossRef]
15. Ouyang, J.; Tang, T.; Yao, J.; Li, M. Active Voltage Control for DFIG-Based Wind Farm Integrated Power System by Coordinating Active and Reactive Powers Under Wind Speed Variations. *IEEE Trans. Energy Convers.* **2019**, *34*, 1504–1511. [CrossRef]
16. Moursi, M.; Joos, G.; Abbey, C. A Secondary Voltage Control Strategy for Transmission Level Interconnection of Wind Generation. *IEEE Trans. Power Electr.* **2008**, *23*, 1178–1190. [CrossRef]
17. Xu, G.; Xu, L.; Morrow, D.; Chen, D. Coordinated DC Voltage Control of Wind Turbine with Embedded Energy Storage System. *IEEE Trans. Energy Convers.* **2012**, *27*, 1036–1045. [CrossRef]
18. Yao, J.; Li, H.; Liao, Y.; Chen, Z. An Improved Control Strategy of Limiting the DC-Link Voltage Fluctuation for a Doubly Fed Induction Wind Generator. *IEEE Trans. Power Electr.* **2008**, *23*, 1205–1213.
19. Zhu, D.; Ma, Y.; Li, X.; Fan, L.; Tang, B.; Kang, Y. Transient Stability Analysis and Damping Enhanced Control of Grid-Forming Wind Turbines Considering Current Saturation Procedure. *IEEE Trans. Energy Convers.* **2024**, 1–11. [CrossRef]
20. He, D.; Shi, G.; Peng, S.; Cai, X. Analysis on the Operation Characteristics of Series Connected DC Based Wind Farm. *South. Power Syst. Technol.* **2012**, *6*, 95–99. (In Chinese)
21. He, D.; Shi, G.; Wu, G.; Cai, X. The Control Strategy of DC Series-Type Wind Turbines and Its Simulation. *South. Power Syst. Technol.* **2012**, *6*, 100–104. (In Chinese)
22. Shi, G.; Wang, Z.; Zhu, M.; Cai, X. Variable speed control of series-connected DC wind turbines based on generalized dynamic model. In Proceedings of the 2nd IET Renewable Power Generation Conference, Beijing, China, 9–11 September 2013.
23. Lee, L.; Yoo, Y.; Yoon, M.; Jang, G. Advanced Fault Ride-Through Strategy by an MMC HVDC Transmission for Off-Shore Wind Farm Interconnection. *Appl. Sci.* **2019**, *9*, 2522. [CrossRef]
24. Yao, L.; Shi, G.; Cao, Y.; Wang, Z.; Zhu, M.; Cai, X. Variable Speed Control of Series-Connected DC Wind Turbines in the Internal Grid of Offshore DC Wind Farm. *Power Syst. Technol.* **2014**, *38*, 2410–2415. (In Chinese)
25. Beik, O.; Al-Adsani, A. A Wind Turbine Generator Design and Optimization for DC Collector Grids. *IEEE J. Emerg. Sel. Top. Power Electron.* **2022**, *10*, 484–493. [CrossRef]
26. Liu, Z.; Cheng, X.; Peng, X.; Wang, P.; Zhao, X.; Liu, J.; Jiang, D.; Qu, R. A review of common-mode voltage suppression methods in wind power generation. *Renew. Sust. Energ. Rev.* **2024**, *203*, 114773. [CrossRef]
27. Rong, F.; Wu, G.; Li, X.; Huang, S.; Zhou, B. ALL-DC Offshore Wind Farm with Series-Connected Wind Turbines to Overcome Unequal Wind Speeds. *IEEE Trans. Power Electr.* **2019**, *34*, 1370–1381. [CrossRef]

28. Mou, D.; Yuan, L.; Luo, Q.; Li, Y.; Liu, C.; Zheng, J.; Zhao, Z. Overview of Multi-Degree-of-Freedom Modulation Techniques for Dual Active Bridge Converter. *IEEE J. Emerg. Sel. Top. Power Electron.* **2023**, *11*, 5724–5737. [CrossRef]
29. Zumel, P.; Ortega, L.; Lázaro, A.; Fernández, C.; Barrado, A.; Rodríguez, A.; Hernando, M. Modular Dual-Active Bridge Converter Architecture. *IEEE Trans. Ind. Appl.* **2016**, *52*, 2444–2455. [CrossRef]
30. Babaghorbani, B.; Beheshti, M.; Talebi, H. A Lyapunov-based model predictive control strategy in a permanent magnet synchronous generator wind turbine. *Int. J. Electr. Power Energy Sys.* **2021**, *13*, 106972. [CrossRef]
31. Wang, H.; Mou, D.; Ji, S.; Yuan, L.; Zeng, Y.; Zheng, J.; Zhao, Z. Universal Phase-Shift Modulation Scheme and Efficiency Optimization for Modular Multiactive Bridge Converter. *IEEE Trans. Ind. Electron.* **2024**, *71*, 7312–7321. [CrossRef]
32. Lee, S.; Jeung, Y.; Lee, D. Voltage Balancing Control of IPOS Modular Dual Active Bridge DC/DC Converters Based on Hierarchical Sliding Mode Control. *IEEE Access* **2019**, *7*, 9989–9997. [CrossRef]